SF/1

PHYSICS OF LAYER CLOUD AND FOG

by

R. Brown

1. INTRODUCTION

In order to reduce this topic to a reasonable length the discussion will be limited to the physics of a quasi-steady state stratocumulus sheet and the formation, growth and dissipation of radiation fog. Although these topics differ in detail they both involve the interaction of radiation and turbulence, with the microphysics playing a relatively passive role, except in the determination of the visibility and the growth of precipitation-size drops. The latter process is not discussed further here.

The distinction between stratocumulus and stratus is rather a grey area which will not be pursued further. For the purposes of this discussion stratocumulus is taken to be that layer cloud forming beneath an inversion associated with anti-cyclonic subsidence. The formation of stratocumulus is associated with the cooling and/or moistening of the boundary layer. It can also form from the spreading out of cumulus under the subsidence inversion.

2. PHYSICS OF STRATOCUMULUS

2.1 General Features of Stratocumulus

The stratocumulus-capped boundary layer is basically convective, the convection being driven by longwave radiative loss from the cloud top and heating at the surface. The latter is important over land during the day and over a warm sea.

The basic structure of stratocumulus is well illustrated by recent measurements made at RAE Cardington using a tethered balloon. Figure 1 shows measured profiles of temperature and humidity mixing ratio through a sheet of nocturnal stratocumulus. A dry adiabatic lapse rate extended from close to the surface to the cloud base where it changed to a wet adiabatic lapse rate. (The unbroken line on Figure 1 marks the dry and wet adiabatic lapse rate). The surface-based inversion is a feature sometimes associated with nocturnal stratocumulus. Otherwise the boundary layer was well mixed with respect to temperature. The humidity mixing ratio tended to decrease with height. This was often more noticeable than on the profile shown in Figure 1.

At the cloud top there was a marked inversion of temperature and lapse of humidity mixing ratio. This is in good agreement with a summary of earlier observations produced by Cornford (1966). For example he quotes the observations of James (1959) who found inversions of up to $8^{\circ}C$ across the 100 m above cloud top. However the recent balloon observations have a much higher vertical resolution than the earlier aircraft data and have shown that a $4^{\circ}C$ temperature inversion can occur over 1 to 10 m above cloud top. The cloud top was coincident with the base of the inversion to within the accuracy of the measurements (4 m). The minimum of humidity mixing ratio often occurs up to 100 m above cloud top, although this feature is not evident on the profile in Figure 1. As yet there is no tenable explanation for this phenomenon.

2.2 Cloud Radiative Properties

A typical value for the net longwave radiative loss from the cloud top is 60-100 Wm^{-2}, if there is clear sky above. The resultant divergence of net longwave flux, occurring typically over a depth of 50 m beneath cloud top, leads to radiative cooling rates of 5 to 10 $^{o}C\ hr^{-1}$. This is illustrated in Figure 2. The dots and crosses are observations and the unbroken lines theoretical values from a longwave radiative transfer scheme (Roach and Slingo 1979). Note also that there is a slight warming at cloud base due to absorption of 8-13 μm window radiation from the warmer surface. The longwave radiative cooling rate is a function of cloud liquid water content but is fairly independent of the drop-size distribution.

It is more difficult to summarise the role of solar radiation because of the variation of the incident intensity with zenith angle (ie time of day, latitude, season). Typical values for the downward flux are 1000 Wm^{-2} with the sun overhead, 800 Wm^{-2} U.K. June midday, 400 Wm^{-2} U.K. October midday. The albedo of layer cloud (ie percentage of the incident flux which is reflected back to space) is in the range 40-90% whilst 3-15% of the incident flux is absorbed in the cloud. The absorption increases with cloud thickness but reaches a limiting value of about 20% if precipitation is absent. As the zenith angle increases (ie low sun) the albedo increases and the percentage absorption decreases. There is also some dependence on drop size. With increasing drop size the cloud reflects less and absorbs more solar radiation.

Finally note that whilst solar absorption warms the cloud-capped boundary layer it is not clear that it significantly reduces the turbulent mixing generated by longwave radiative loss (see next section). Figure 3 shows the calculated longwave and solar heating rates in a stratocumulus layer observed during the JASIN project. The zenith angle was 51^{o} and the downward solar flux at cloud top 675 Wm^{-2}. Despite the fact that the solar radiation absorbed by the cloud (47 Wm^{-2}) is roughly comparable to the net longwave loss (65 Wm^{-2}), the longwave cooling over the top $2\frac{1}{2}$ mb of cloud is an order of magnitude larger than the solar heating. This is because the solar absorption is distributed more evenly through the cloud than the longwave loss.

2.3 Generation of Turbulence

The radiative cooling at cloud top leads to the generation of cold descending plumes and compensating warm updraughts. Figure 4 shows an example of high frequency vertical velocity and temperature data obtained at night with the Cardington Turbulence Probe about 50 m beneath cloud top. Prominant cold downdraughts and warm updraughts are marked by arrows. Also shown is the resultant heat flux, ie $\overline{W'T'}$. In the mean there is a net upward flux of heat which tends to offset the radiative cooling so that the observed rate of temperature change beneath cloud top can be much less than the radiative cooling rate (and was $\sim$ 0 on this occasion). The Cardington observations in nocturnal stratocumulus have shown that convection generated by longwave cooling can maintain a well mixed boundary layer of depth 1 km. Of course over land during the day convection can be generated by surface heating as well. Over the ocean the surface can be a source of convective mixing day or night.

Turbulence dies away rapidly in the strong inversion at cloud top so that the air above is generally non-turbulent.

2.4 Entrainment

An important consequence of the turbulence within the cloud is that at the cloud top dry warm air is entrained into the cloud from the inversion. It is extremely difficult to observe this process directly. Figure 5 is a very schematic reconstruction of an entrainment event from turbulence probe data near cloud top. The shaded area represents the cloud top inversion of thickness a few metres. The arrows show the sign of the observed vertical velocity used in the reconstruction.

The entrained air, being warmer than the cloud, represents a downward flux of sensible heat into the cloud. However this is partially offset by the latent heat of evaporation required to saturate the dry entrained air. The predominant effect can be determined from the cloud top step in any variable which is conserved during evaporation eg wet bulb or equivalent potential temperature (θw, θe).

If the entrained air becomes denser than its surroundings it can sink deep into the cloud. It is generally accepted that this will lead to the dispersal of the cloud sheet as the unsaturated air is mixed rapidly through the cloud eg Lilly (1968). A detailed discussion of this topic is given by Randall (1980a) and Deardorff (1980a).

Work is expended during entrainment, against the buoyancy force associated with the cloud top inversion and to give turbulent kinetic energy to the quiescent entrained air. This is drawn from the turbulent kinetic energy of the boundary layer.

The entrainment of air would in the absence of subsidence cause the cloud top to rise. An entrainment velocity (w_e) has been defined by:-

$$we = \frac{dh}{dt} - w_3 \qquad (1)$$

where $\frac{dh}{dt}$ is the rate of change of cloud top height following the motion and w_s is the subsidence velocity eg Lilly (1968), Deardorff (1976). Then the flux of sensible heat into the cloud top due to entrainment is given by $w_e \Delta\theta$ where $\Delta\theta$ is the potential temperature step at cloud top. Since it does not appear feasible to measure the entrained heat flux directly equation (1) appears to offer a method of indirect determination. Unfortunately except in special circumstances it is not possible to evaluate Ws with any degree of accuracy and it can be difficult to evaluate $\frac{dh}{dt}$ if the cloud top is undulating. On one occasion at Cardington the data allowed an estimate to be made of w_e of 0.5 cm s^{-1}. This is within the range of the theoretical values calculated by Deardorff (1976).

2.5 Flux Profiles and Energy Budget

Figure 6 shows an example of sensible (F_h) and latent heat flux (E_w) profiles and net longwave flux (F_N) profile measured or inferred from observations in nocturnal stratocumulus. Upward fluxes are positive. The negative surface heat flux results from a surface-based inversion. Over land during the day the sensible heat flux would be positive ($\sim$ 50 Wm^{-2}). Model calculations have shown that over the sea the surface sensible heat flux can be positive or negative for an equilibrium cloud sheet.

The large convergence of sensible heat flux between 920 and 905 mb offsets the divergence of net longwave radiation over this interval. The negative value of F_h above 909 mb represents the downward heat flux due to entrainment. The inferred constancy of the water vapour flux indicates that surface evaporation was required to offset the effect of entrainment of dry air at the cloud top.

Whilst a detailed description of the energy budget is not appropriate here a few values are given for reference (assuming $\rho C_p = 1.2 \times 10^3$ Jm^{-3} ^{o}K^{-1}, $\rho L = 3 \times 10^6$ J m^{-3} where ρ, C_p are the density and thermal capacity of air). A cloud top net radiative loss of 67 Wm^{-2} would cause a 1 km deep boundary layer to cool 1^{o}C in five hours if not offset by other terms. This implies that the local heat storage term must be measured accurately in energy budget studies. A potential temperature gradient of 1^{o}C/100 km with a mean windspeed of 7m s^{-1} would represent a heat gain or loss of 84W m^{-2} over a 1 km boundary layer. Again this is a significant term which must be taken into account and suggests that two-dimensional measurements are required for budget studies. In fact measurements on one night at Cardington, when the local heat storage term was negligible, showed that the net radiative loss from the cloud top could only be balanced locally by advection. This need not be so over land during the day because of the upward directed sensible heat flux and solar absorption. If the entrainment velocity is 0.5 cm s^{-1} and the cloud top potential temperature and humidity mixing ratio steps +5^{o}C and -1.5g Kg^{-1} respectively, then $w_e \Delta\theta \simeq +30$W m^{-2}, $w_e \Delta q \simeq -22.5$ W m^{-2}. In this case evaporative cooling largely offsets the sensible heat gain so that there is a net gain of 7.5 W m^{-2}.

2.6 Cloud Liquid Water Content and Microphysical Structure

In a well mixed boundary layer without entrainment the humidity mixing ratio above cloud base would be constrained to be the saturation value at the local temperature. It would therefore decrease with height at a rate determined by the wet adiabatic lapse rate. The total water content would be independent of height, since it is a conservative quantity. Therefore the liquid water content would increase roughly linearly with height at the adiabatic value of about 1 g m^{-3} Km^{-1}. Observations show that in stratocumulus the liquid water content does increase roughly linearly with height but at $\frac{1}{2}/\frac{2}{3}$ of the adiabatic rate eg Cornford (1966). Departures from the adiabatic value are almost certainly caused by the entrainment of dry air from above the cloud.

Figure 7 shows typical observations of liquid water content and drop concentration from one ascent through a stratocumulus layer. The dashed line on the liquid water content profile is the adiabatic value. The central diagram shows isopleths of the percentage of drops per unit radius interval. Thus the maximum isopleth shows the mode of the drop-size distribution. This moves towards larger radii with increasing height. The drop concentration shows no trend with height. The overall picture is consistent with the peak super-saturation being close to cloud base. Thus the concentration of activated droplets is established close to cloud base and thereafter the increase of liquid water content with height is brought about by condensation on the pre-existing drops.

2.7 Stratocumulus Models

The pioneering work on stratocumulus modelling is due to Lilly (1968) and this has been extended by Deardorff (1967) and Schubert et al (1979). These are analytic models in which the boundary layer is assumed to be well mixed so that θ_w and the total water mixing ratio (q_w) are constant with height. The latter assumption is less well borne out by observations than the former. Steady state

solutions are sought by Lilly in terms of net radiative loss from cloud top and subsidence rate. Schubert et al have extended Lilly's model to look for horizontally inhomogenous solutions eg sea surface temperature changing downwind. Deardorff (1976) has looked in detail at the factors governing the entrainment velocity and the rate of change of cloud thickness. Deardorff (1980b) has also developed a three dimensional numerical model which explicitly calculates the turbulent eddy structure down to a scale of 50 m.

The complexity of these models precludes a detailed discussion here but some results will be given and unresolved problems noted. The model complexity partly arises from the necessity to use two thermodynamic variables in the moist boundary layer. The conservative variable with condensation is θ_w or θ_e. However the generation of turbulent kinetic energy by buoyancy is related to the virtual potential temperature flux $(w'\theta_v')$ where $\theta_v = \theta \left[1 + 0.61q - q_L \right]$. q_L is the liquid water mixing ratio and this term allows for the drag of the liquid water.

A central problem of all analytic models is the formulation of the entrainment fluxes. The entrainment velocity can be related to the cloud top virtual potential temperature flux $(w' \theta'_v)_h$, since turbulent kinetic energy is expended in entraining the stable, non-turbulent air from above. Unfortunately $(w'\theta_v')_h$ cannot be calculated explicitly and some assumption is required to close the equation set. $(w'\theta v')_h$ is often taken to be a prescribed fraction of the surface value or of $\int_0^h (w'\theta_v') \, dz$. The rationale for these choices depends upon consideration of the turbulent kinetic energy budget and is not discussed further here. [See Ball (1960), Lilly (1968), Randall (1980b)].

Using the integral assumption Deardorff (1976) finds that entrainment is promoted by upward fluxes of heat and water vapour at the surface, by longwave radiative loss and by small jumps in temperature and total water mixing ratio at the cloud top. He also investigates factors governing the rate of change of cloud thickness following the motion. The cloud is thickened by longwave loss, surface evaporation and by entrainment if the cloud top steps in temperature and humidity are not too large. With large jumps the entrained air can be so warm and dry that the cloud base rises faster than the cloud top leading to eventual dispersal. Schubert et al (1979) have shown that the equilibrium cloud top and base height decreases with increasing subsidence velocity and decreasing sea surface temperature. They also investigated the change in cloud structure when a cloud-capped boundary layer in equilibrium encountered a $+2^{\circ}C$ step in surface temperature. The cloud top was still rising 2000 km downstream although the cloud base adjusted more quickly. If this time constant is typical then one should not expect to be able to relate the local stratocumulus structure to the local boundary conditions alone.

Finally it should be noted that many of these models make controversial assumptions that are still being debated in the literature, especially with respect to the treatment of radiation at the cloud top. The relationship between the assumed net flux profile, cloud top and inversion base is discussed by Kahn and Businger (1979), Lilly and Schubert (1980), Randell (1980b). Lilly (1968) put all the radiative flux divergence in an infinitessimaly thin layer at cloud top so that no radiative cooling was available to produce turbulence in the cloud. Deardorff (1976) put a fraction of the divergence in the turbulent boundary layer but assumed a linear profile. Kahn and Businger (1979) have suggested that most of the flux divergence should occur beneath the cloud top ie as in the profile illustrated in Figure 2. However the problem is complicated by undulations in the cloud top. Should one use a radiation profile measured from the local cloud top or an ensemble average profile which smears out the detail of the cloud top structure? At the present time further observations are required to inform the modelling effort.

3. PHYSICS OF FOG

3.1 Fog Formation Processes

Many types of fog are discussed in the literature eg Jiusto (1980) suggests 15 types have been mentioned. Some of these are described briefly below and then the physics of radiation fog is discussed in detail.

Warm Advection Fog forms when warm air flows over a colder surface. It has a high liquid water content (up to 1 g m^{-3}), can cover large areas and is stable.

Cold Advection Fog forms when cold air flows over a warmer surface. According to Lee (1975) it has a low liquid water content ($\sim$ 0.01 g m^{-3}) and is shallow. However the observations of Pilie et al (1979) and the model of Oliver et al (1978) suggest that such fog can also attain a substantial depth and liquid water content.

Mixing Fog has been reported by Lee (1975) to occur when the windfield interacts with the coastal topography to produce a region of high turbulent mixing over the sea. He claims enhanced evaporation cools the ocean surface to produce fog.

Low Level Convergence. Pilie et al (1979) have observed fog to form offshore in a region of low level convergence, again caused by the interaction of the windfield with the coastal topography.

Lowering of Stratus. This is favoured by low windspeed according to Barker (1973). It also occurs at night when the longwave loss from the cloud top is no longer partially offset by solar absorption. According to Oliver et al the cloud base only reaches the surface if the cloud top is below 400 m.

3.2 Formation of Radiation Fog

The following picture of the formation and growth of radiation fog has emerged from a combination of observations and modelling eg Stewart (1955), Roach et al (1976), Brown and Roach (1976), Lala et al (1975). On a radiation night the ground cools by radiating to space mainly through the atmospheric window, a typical value of the surface net longwave flux being 55-75w m^{-2} in the United Kingdom. The surface temperature initially falls rapidly but then more slowly as the radiative loss is partially offset by heat conducted upwards through the soil as a result of the temperature gradient established within the top few centimetres. A typical value for this soil heat flux, measured at a depth of 4 cm is 20 - 30w m^{-2}. The turbulent fluxes of sensible and latent heat only make a small contribution to the surface energy balance because of the low level of mixing with light winds and a strong inversion.

As the surface cools the air in the lowest few metres radiates directly to the colder ground. The radiative cooling rate in this region can reach 1 or 2°C hr^{-1} compared to a typical value well removed from the surface of 0.1-0.2°C hr^{-1}. Once the air at the surface becomes saturated, further cooling leads to dew deposition and hence a drying of the air. Whether fog now forms depends upon a balance between radiative cooling leading to saturation of the air and turbulent diffusion which although it may be cooling the air is also drying it. Both model results and observations show that radiation fog forms more readily with a low level of turbulent mixing. This is illustrated in Figure 8 by results from a numerical model. At the top are the exchange coefficient profiles associated with the model I-IV temperature and liquid water content profiles

presented beneath. Model IV used only molecular diffusion and fog formed earliest in this case. The model results of Brown and Roach and of Lala et al agree that K $\sim$ 0.01 m^2 s^{-1} for fog formation on a realistic time scale. The field studies of Roach et al suggested that fog formed when the air was close to saturation and the surface wind fell below 1 m s^{-1}. This ties in with the observations of Monteith (1957) that on a radiation night if the 2 m wind fell below 0.5 m s^{-1} there was an abrupt decrease in the rate of dew deposition. He suggested this was caused by the virtual cessation of turbulent transfer under these conditions. Since radiative cooling of the air will continue condensation must eventually take place directly into the air.

The mechanism by which mixing of damp air masses of a different temperature produces supersaturation and hence fog does not appear to be significant for radiation fog. This is probably because the temperature differences of the parcels than can be mixed by light winds on a radiation night are too small. It is necessary to mix two saturated parcels with a temperature difference of about 5°C to produce a liquid water content of 0.1 g m^{-3}, typical of radiation fog. Brown and Roach (1976) found that their model could not produce fog on a realistic time scale if the radiative cooling of the air was removed. It is interesting to note that both Barker (1973) and Oliver et al (1978) suggest that radiation plays an important role in the formation and growth of advection fog.

3.3 Development of the Mature Fog

As the fog increases in depth and liquid water content radiative cooling by the fog drops becomes dominant in the upper part of the fog. With the increasing optical depth of the fog the radiative loss from the surface is reduced to a value below that of the soil heat flux and the surface temperature starts to rise. The inversion then lifts from the surface where it is replaced by a superadiabatic lapse rate. This process is illustrated by the model III and IV numerical simulations shown in Figure 8. Both model results and observations show that the inversion starts to lift from the surface when the fog is 20 to 50 m deep.

Figure 9 shows the observed temperature and net longwave flux profile through a deep mature fog. The inversion has lifted to become almost coincident with the fog top, although it is not as sharp as at the top of stratocumulus. The radiative cooling rate calculated from the net flux profile is also shown. This is lower than that observed in stratocumulus eg Figure 2 because of the lower liquid water content typical of radiation fog. However the cooling at the fog top combined with the warming at the surface produces weak convection and Figure 9 shows a wet adiabatic lapse rate throughout most of the fog. The observations of Pilie et al (1979) and the model of Oliver et al (1978) have shown that radiative loss from the top of advection fog also generates an inversion at the fog top.

Recent observations at Cardington suggest that besides having a strong effect on the thermal structure of the boundary layer, fog also modifies the windfield, with the region of strongest windshear migrating from the surface towards the fog top. This has been confirmed by an extended version of the model of Brown and Roach which includes the solution of the momentum equations, using exchange coefficients which are functions of the local Richardson number. This effect could enhance mixing at the fog top.

3.4 Dispersal of Radiation Fog

Radiation fog may be dispersed by increasing gradient wind, by the advection of cloud cover and by solar radiation.

Analysis of the Cardington fog project data suggests that increasing gradient wind causes an increase in windshear through the fog top. This enhances the mixing of drier air into the fog and in the limited number of cases analysed led to the dispersal of the fog from the top first.

Saunders (1960) has drawn attention to the effectiveness of the advection of a cloud sheet in dispersing an existing radiation fog. He found that the lower the cloud the more rapid was the fog clearance. The ability of clouds to clear fog also seemed related to the soil-air temperature gradient with large gradients enhancing fog clearance. This latter result was related by Saunders to the role of the soil heat flux in dispersing the fog. The mean dispersal time from all Saunders observations was 2.2 hours.

Figure 10 shows the temperature and liquid water content profiles from a numerical simulation of the clearance of fog by cloud. A cloud sheet more than a few hundred metres thick will have an emissivity approaching unity and so will produce a downward flux in the atmospheric window approximately equal to the black body flux at the cloud base temperature. The cloud has been introduced into the model at time t by increasing the downward flux in the atmospheric window from above the top boundary of the model. This significantly reduces the net longwave loss from the fog. For example in the model integration illustrated in Figure 10 the radiative cooling near the fog top was reduced from $5^{\circ}C\ hr^{-1}$ to $0.3^{\circ}C\ hr^{-1}$ by the appearance of cloud. However the surface continued to be warmed by the soil heat flux and the upward diffusion of heat from the surface warmed the air and reduced the fog liquid water content. In the example illustrated in Figure 10 the fog has nearly cleared two hours after the appearance of cloud. Note that a net input of heat of 10 w m^{-2} into a fog of depth 50 m and liquid water content 0.2 g m^{-3} will evaporate it in about 40 minutes.

Solar radiation is generally less effective at dispersing fog than cloud because the fog top net longwave loss continues undiminished. During the United Kingdom fog season direct absorption of solar radiation in the fog will be small compared to the longwave loss. Although accurate calculations have yet to be performed for radiation fog, the direct absorption is unlikely to exceed 2-3%. The maximum downward solar flux in the United Kingdom in early December is $\sim$ 300 w m^{-2}, giving a figure for the direct absorption around 10 w m^{-2}, but only several hours after sunrise. Thus the fog can continue to grow upwards after sunrise, driven by the longwave loss. The mode of clearance is by heating of the surface by absorption of the solar radiation and turbulent transport of the heat to the air. This suggests that clearance will commence at the surface and this is often observed to happen.

It is commonly believed that fog thickens around sunrise because of enhanced turbulence. The classical mixing mechanism is generally assumed to be responsible. It is likely that the release of water vapour from the warming surface is an important factor.

3.5 Radiation Fog Microphysics

The pre-fog radiative cooling rates of 1-2°C hr^{-1} are equivalent to very low ascent rates of 5 cm s^{-1}. Thus the peak supersaturation in radiation fog is believed to be low $\sim$ 0.05 - 0.1% eg Brown (1980), Meyer et al (1980). For a given CCN distribution a lower concentration of nuclei will be activated in fog than in stratocumulus or cumulus.

The visibility in fog is influenced by the CCN concentration and the model results of Brown (1980) have shown that the minimum visibility $\propto \frac{1}{\sqrt[3]{n}}$ where n is the CCN concentration. The CCN concentration influences the visibility by its effect on the drop-size distribution. As the CCN concentration is increased a higherconcentration of activated drops are formed and competition for the available water reduces the mean drop radius. This is illustrated by the model results shown in Figure 11. The drop-size distributions are shown which result from increasing the basic CCN concentration by a factor of $2\frac{1}{2}$ and 5. These have a higher drop concentration and lower mean radius. The effect on visibility (V) can be demonstrated by a simple calculation assuming a monodisperse drop-size distribution. From Koschmeider's theory

$$V = \frac{3.0}{2\pi N r^2} \qquad (2)$$

The liquid water content is given by

$$W = \tfrac{4}{3}\pi \rho_L N r^3 \qquad (3)$$

where N is the drop concentration and ρ_L the density of water.

Combining (2) and (3)

$$V = \frac{2\rho_L r}{W} \qquad (4)$$

For a given liquid water content reducing r decreases the visibility.

The microphysical fog model tends to give a mean radius which is larger than that shown by the majority of the observations. This is probably because the model underestimates the mixing at the top of a mature fog since it uses exchange coefficients which are constant in time. This implies that the entrainment of drier air and fresh nuclei at the fog top can lead to a reduction in the mean drop radius.

There does not appear to be a concensus opinion about the variation of liquid water content and drop-size distribution with height in radiation fog. Jiusto (1980) reports observations which show liquid water content decreasing

with height in shallow fogs but increasing with height in deep fogs. The Cardington observations have generally shown no trend or a decrease of liquid water content and mean drop radius with height, even in deep fogs. It is necessary to explain these differences before it can be claimed that the physics of radiation fog is completely understood.

Roach (1976) has shown that the net radiative loss from the drops, besides cooling the drops and hence the air by conduction, also fundamentally alters their growth rate. This led him to modify the classical growth equation by the addition of a term representing radiative exchange with the atmosphere. Whilst all other terms in the growth equation decrease with increasing drop radius, the radiative term increases becoming roughly constant at 15 μm radius. Thus radiative exchange dominates the growth of the larger drops in layer cloud and fog.

References - Stratocumulus

Ball F K 1960 Control of inversion height by surface heating. Quart.J.R.Met.Soc., 86, 483-414.

Cornford S G 1966 Stratocumulus - a review of some physical aspects. Met.Mag., 95, 292-303.

Deardorff J W 1976 On the entrainment rate of a stratocumulus capped mixed layer. Quart.J.R.Met.Soc., 102, 563-583.

1980a Cloud top entrainment instability. J.Atm.Sci., 37, 131-147.

1980b Stratocumulus - capped mixed layers derived from a three-dimensional model. Boun.Layer Met., 18, 495-527.

James D G 1959 Observations from aircraft of temperatures and humidities near stratocumulus clouds. Quart.J.R.Met.Soc., 85, 120-130.

Kahn P H and Businger J A 1979 The effect of radiative flux divergence on the entrainment of a saturated convective boundary layer. Quart.J.R.Met.Soc., 105, 303-306.

Lilly D K 1968 Models of cloud capped mixed layers under a strong inversion. Quart.J.R.Met.Soc., 94, 292-309.

Lilly D K and Schubert W H 1980 The effect of radiative cooling in a cloud-topped mixed layer. J.Atm.Sci., 37, 482-487.

Randall D A 1980a Conditional instability of the first kind upside-down. J.Atm.Sci., 37, 125-130.

1980b Entrainment into a stratocumulus layer with distributed radiative cooling. J.Atm.Sci., 37, 148-159.

Roach W T and Slingo A 1979 A high resolution infrared radiative transfer scheme to study the interaction of radiation with cloud. Quart.J.R.Met.Soc., 105, 603-614.

Schubert W H, Wakefield J S, Steiner E J and Cox S J 1979 Marine stratocumulus convection. Part I Governing equations and horizontally homogeneous solutions. J.Atm.Sci., 36, 1286-1307.

Marine stratocumulus convection. Part II Horizontally inhomogeneous solutions. Ibid., 1308-1324.

References - Fog

Barker E H 1973 Oceanic fog - a numerical study. Monterey Cal. Nav. Postgrad. School. Environment Prediction Research Facility, Tech. Pap. 6-73.

Brown R 1980 A numerical study of radiation fog with an explicit formulation of the microphysics. Quart.J.R.Met.Soc., 106, 781-802.

Brown R and Roach W T 1976 The physics of radiation fog: II - a numerical study. Ibid., 102, 335-354.

Jiusto J E 1980 Fog structure. Atmos.Sci.Res.Centre, New York Cloud Physics Lab., Pub. No. 745.

Lala G G, Mandel E and Jiusto J E 1975 A numerical evaluation of radiation fog variables. J.Atm.Sci., 32, 720-728.

Lee S C 1975 Marine Fog Studies. Univ.Missouri, Tech.Rep.No. N00014-75-C-0180.

Meyer M B, Jiusto J E and Lala G G 1980 Measurements of visual range and radiation fog (Haze) microphysics. J.Atm.Sci., 37, 622-629.

Monteith J L 1957 Dew. Quart.J.R.Met.Soc., 83, 322-341.

Oliver D A, Lewellen W S, and Williamson G G 1978 The interaction between turbulent and radiative transport in the development of fog and low-level stratus. J.Atm.Sic., 35, 301-316.

Pilie R J, Mack E J, Rogers C W, Katz U and Kockmond W C 1979 The formation of marine fog and the development of the fog-stratus system along the California coast. J.Appl.Met., 18, 1275-1286.

Roach W T 1976 On the effect of radiative exchange on the growth by condensation of a cloud or fog droplet. Quart.J.R.Met.Soc., 102, 361-372.

Roach W T, Brown R, Caughey S J, Garland J A and Readings C J 1976 The physics of radiation fog: I - a field study. Ibid, 102, 313-333.

Saunders W E 1960 The clearance of water fog following the arrival of a cloud sheet during the night. Met.Mag., 89, 8-10.

Stewart K H 1955 Radiation fogs: 'Investigations at Cardington 1951-54 Air Ministry Met. Research Committee' MRP 912

FIGURE 1

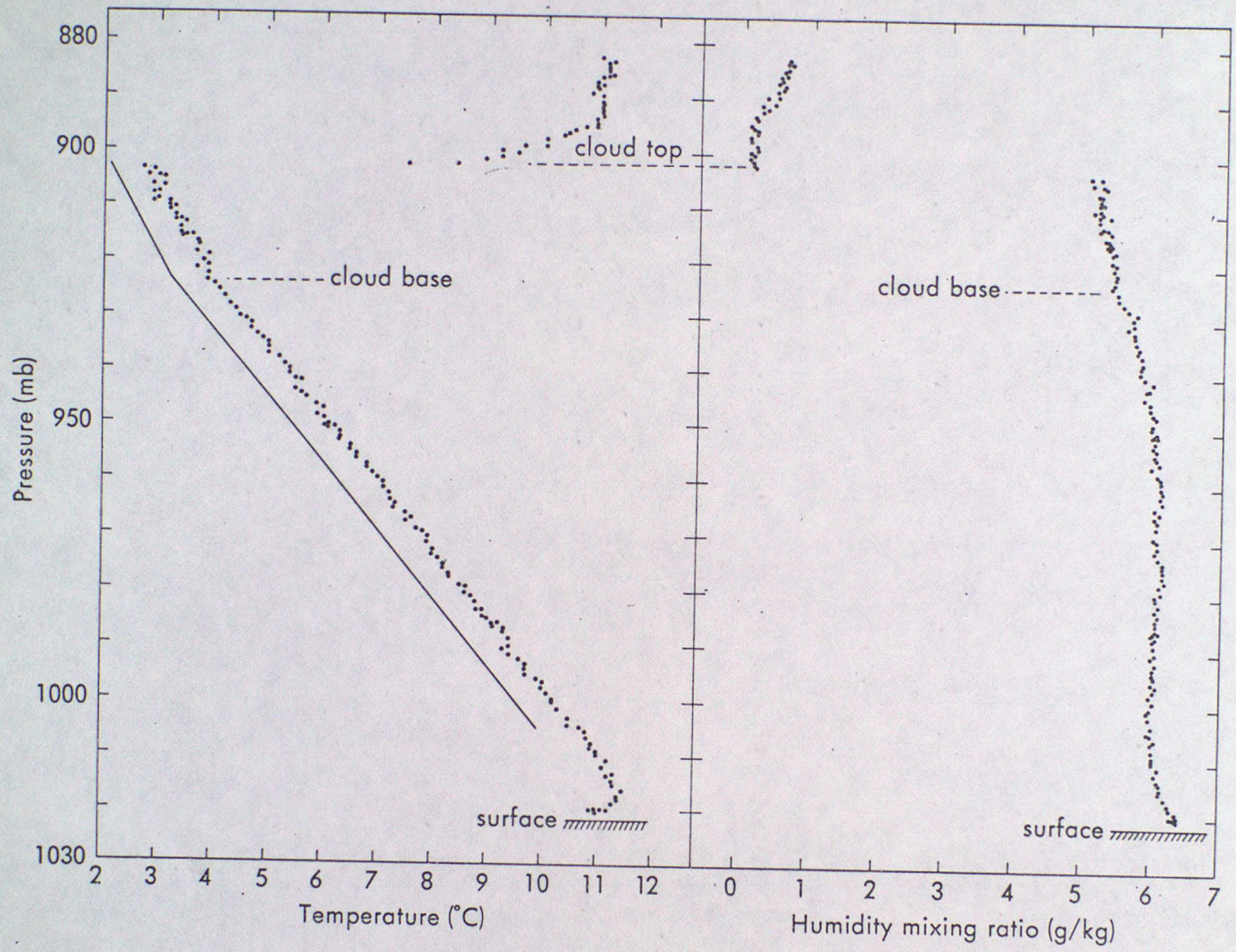
880
900
950
1000
1030
Pressure (mb)
cloud top
cloud base
surface
2 3 4 5 6 7 8 9 10 11 12
Temperature (°C)
cloud base
surface
0 1 2 3 4 5 6 7
Humidity mixing ratio (g/kg)

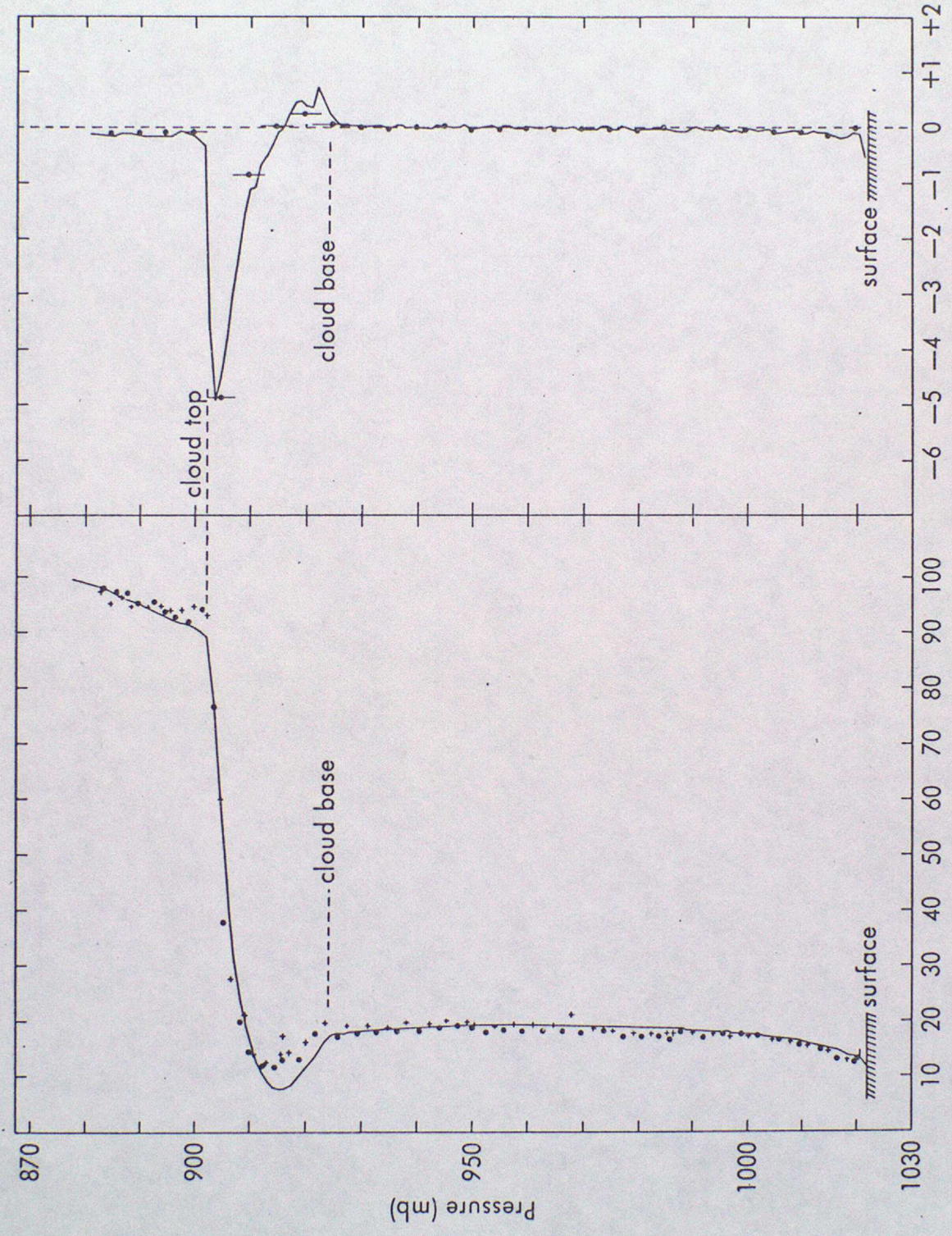
cloud top
cloud base
surface
cloud base
surface
Pressure (mb)
870
900
950
1000
1030
10 20 30 40 50 60 70 80 90 100
Net upward flux (Wm⁻²)
−6 −5 −4 −3 −2 −1 0 +1 +2
Heating rate (°C per hour)

FIGURE 2

FIGURE 3 THEORETICAL LONGWAVE AND SOLAR HEATING RATES IN Sc..

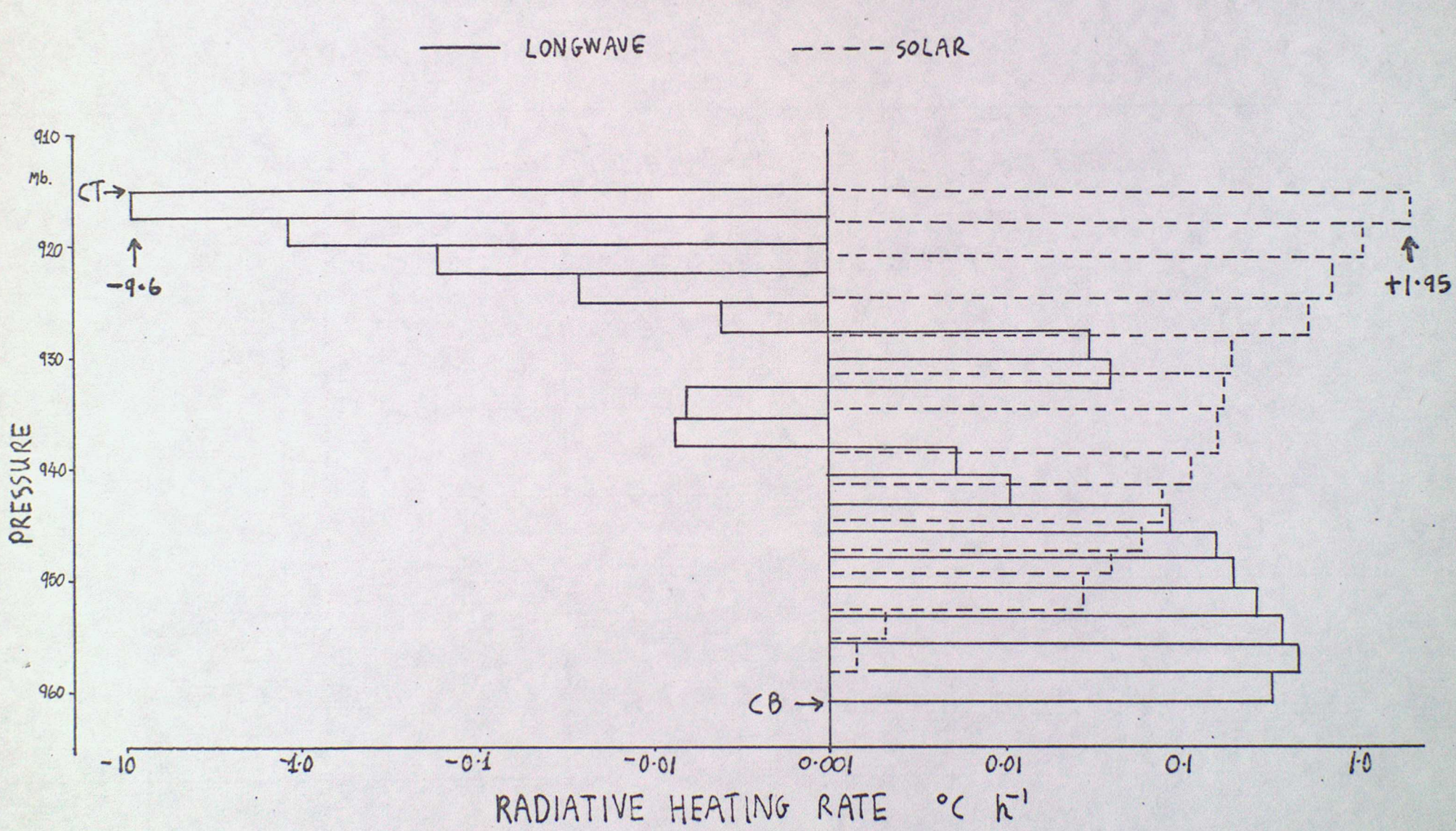

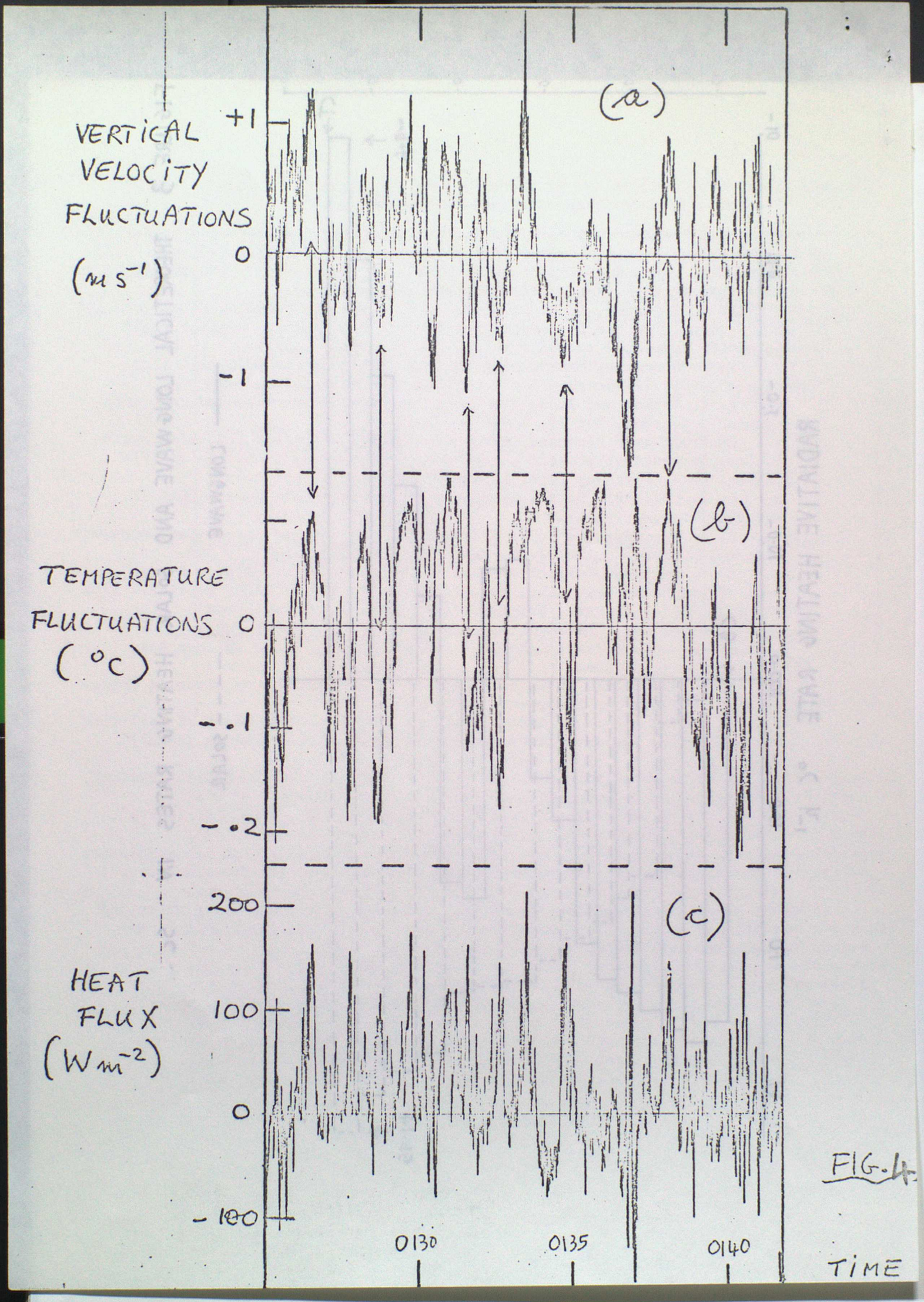
(a)
VERTICAL VELOCITY FLUCTUATIONS (m s⁻¹)
+1
0
-1
(b)
TEMPERATURE FLUCTUATIONS (°C)
0
-.1
-.2
(c)
200
HEAT FLUX (W m⁻²)
100
0
-100
0130
0135
0140
TIME

FIG. 4

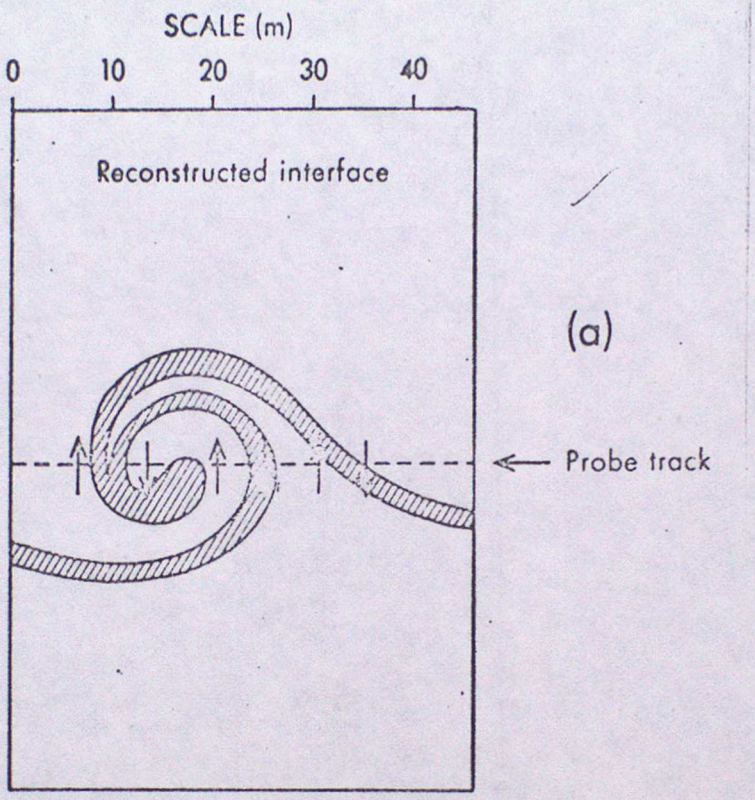

FIGURE 5 Idealised reconstruction of an entrainment event from turbulence probe data. The shaded area represents the cloud top temperature step.

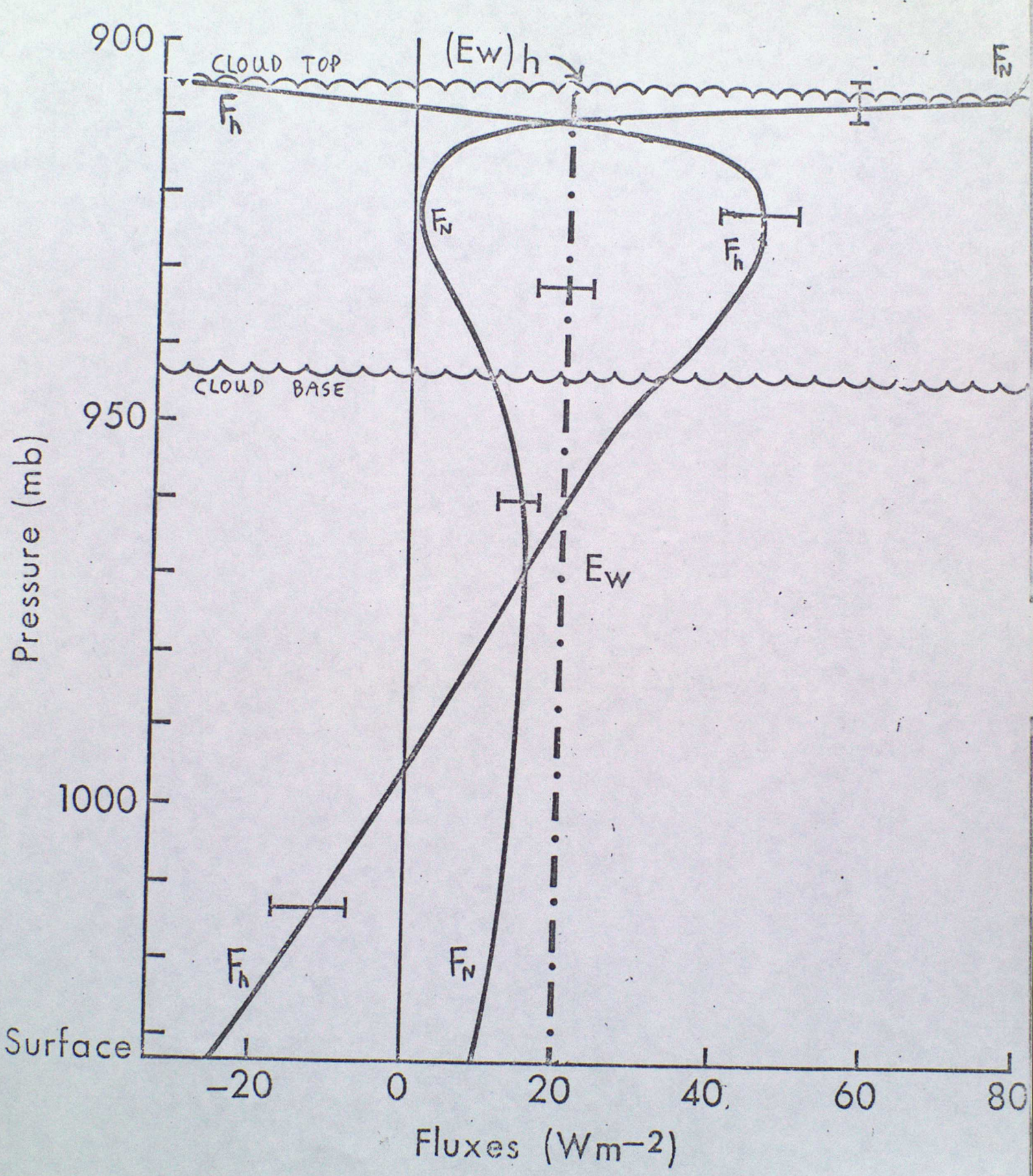

IDEALIZED PROFILES OF SENSIBLE (F_h) AND LATENT (E_w) HEAT FLUXES AND NET LONGWAVE FLUX (F_N) IN NOCTURNAL Sc

FIGURE 6

FIGURE 7

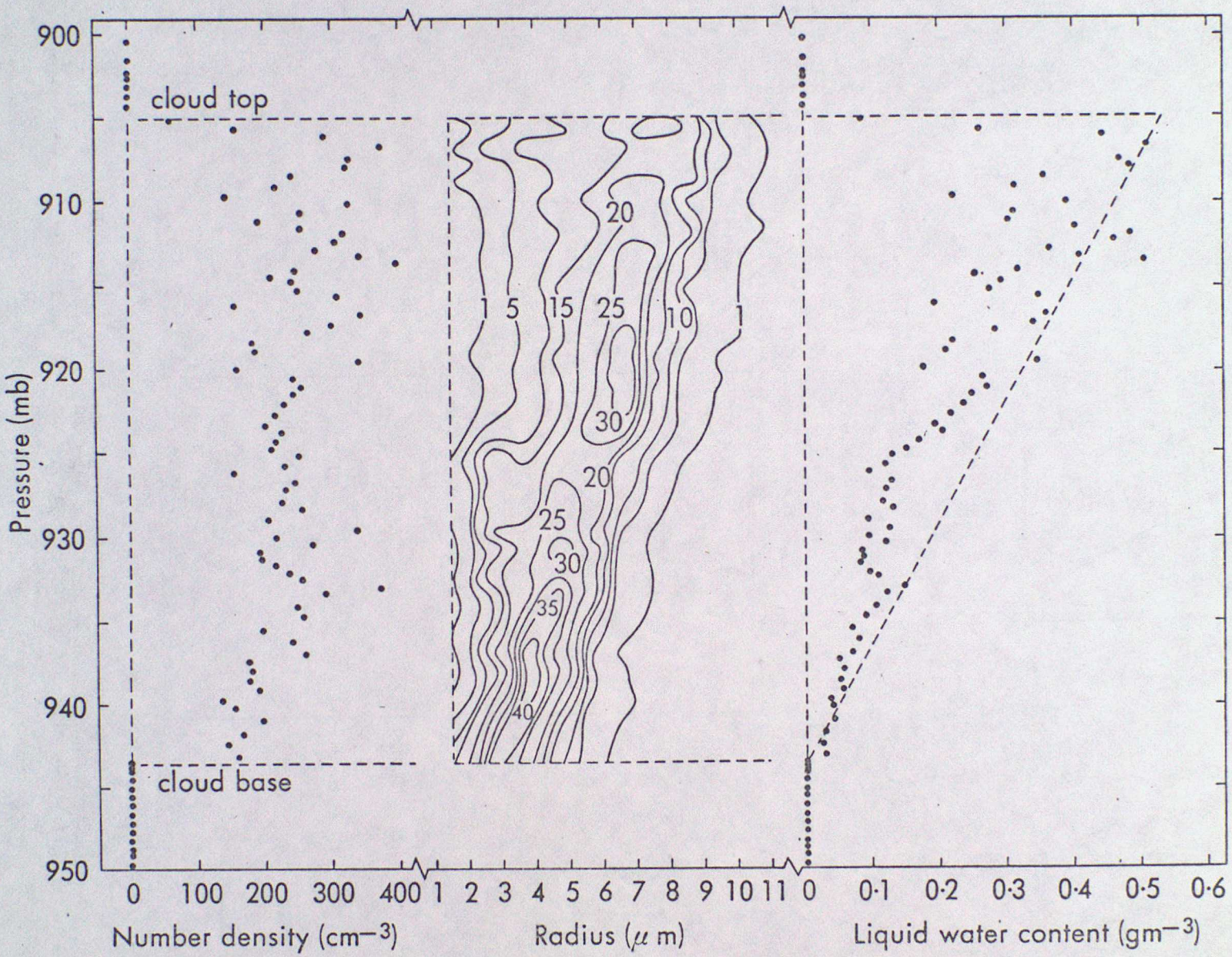
900
910
920
930
940
950
Pressure (mb)
cloud top
cloud base
20
1 5 15 25 10 1
30
20
25
30
35
40
0 100 200 300 400
Number density (cm⁻³)
1 2 3 4 5 6 7 8 9 10 11
Radius (μ m)
0 0·1 0·2 0·3 0·4 0·5 0·6
Liquid water content (gm⁻³)

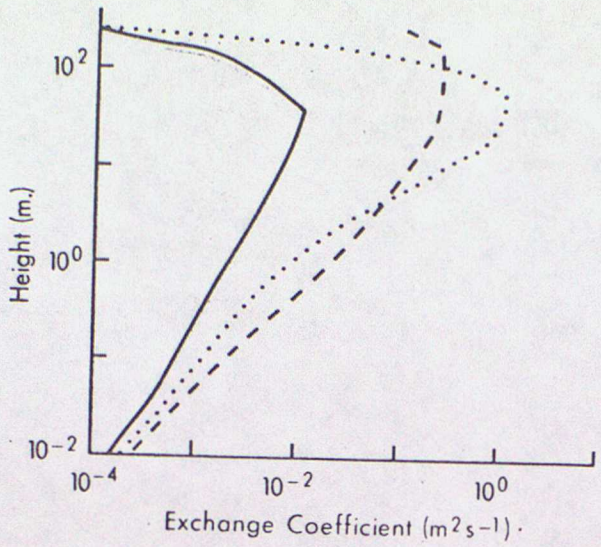

Exchange coefficient regimes ····· Model I; – – – – Model II; ——— Model III.

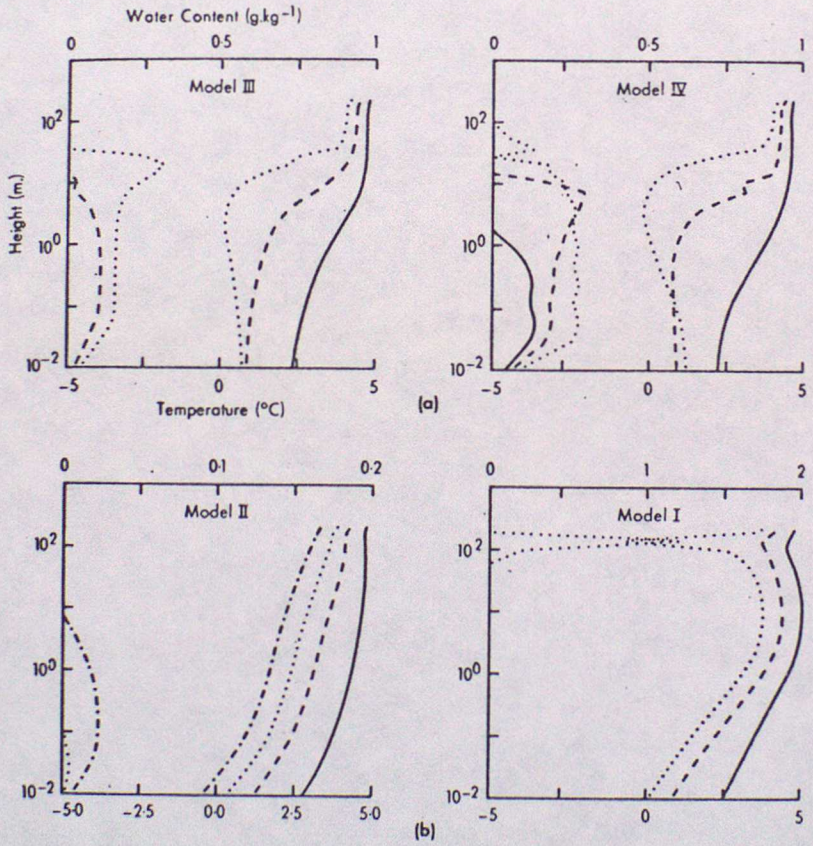

(a) Temperature and liquid water profiles obtained from integrations with model III and model IV exchange coefficient regimes. The profiles are presented at three times from the start of the integration ——— one hour; – – – – three hours; ····· five hours. (b) Temperature and liquid water profiles obtained from integrations with model I and model II exchange coefficient regimes. The profiles are presented at four times from the start of the integration: ——— one hour; – – – – four hours; ····· seven hours; –·–·–·– ten hours.

FIGURE 8

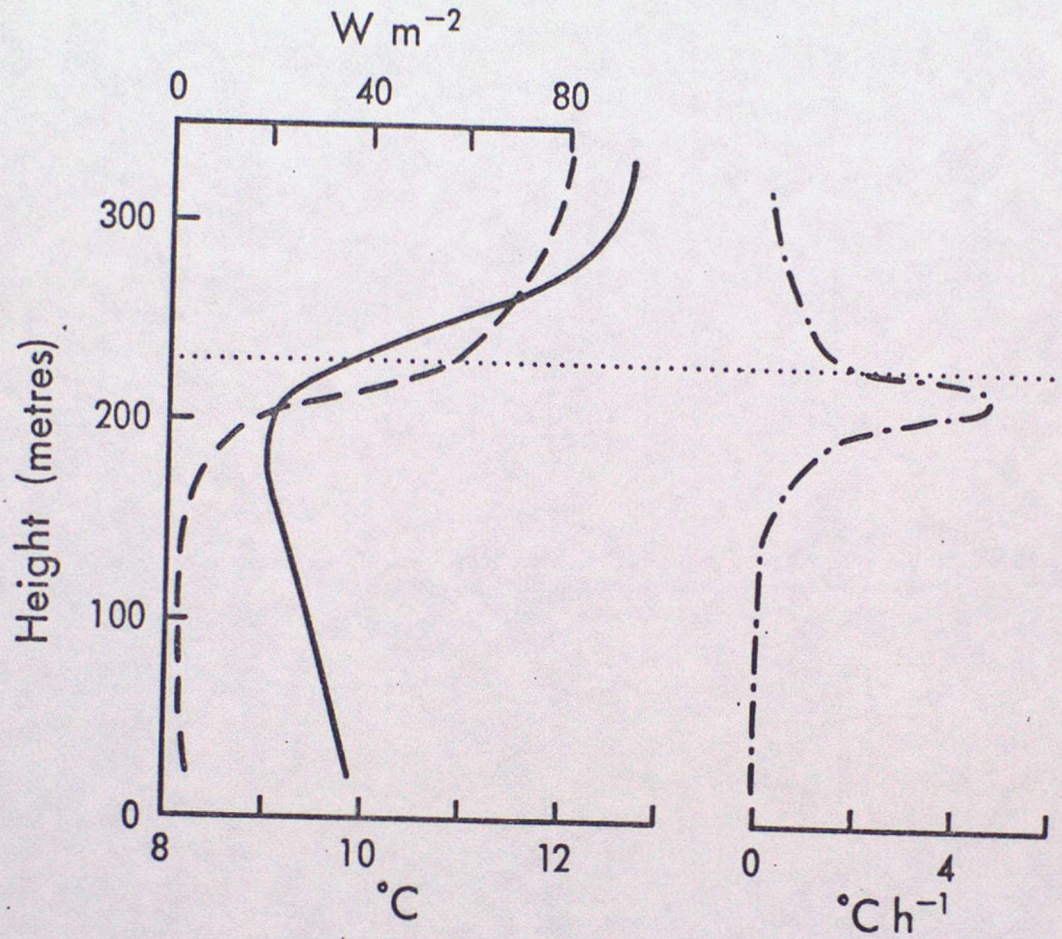

FIGURE 9 Observed profiles of temperature ————————,
net long wave flux - - - - - -
and derived radiative cooling rate -.-.-.-.-.-,
. . . . . FOG TOP

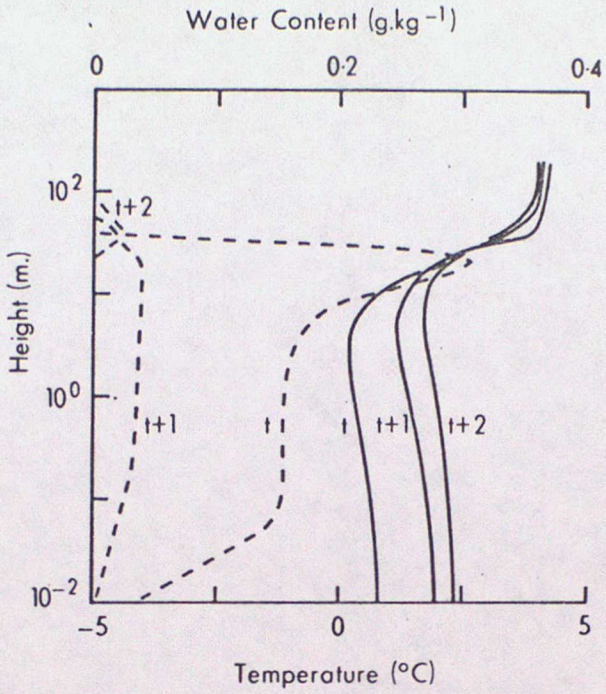

Liquid water content and temperature at times $t + x$ hours where t is the time of advection of cloud cover: - - - - liquid water content; ——— temperature.

FIGURE 10 Model simulation of the clearance of radiation fog by cloud.

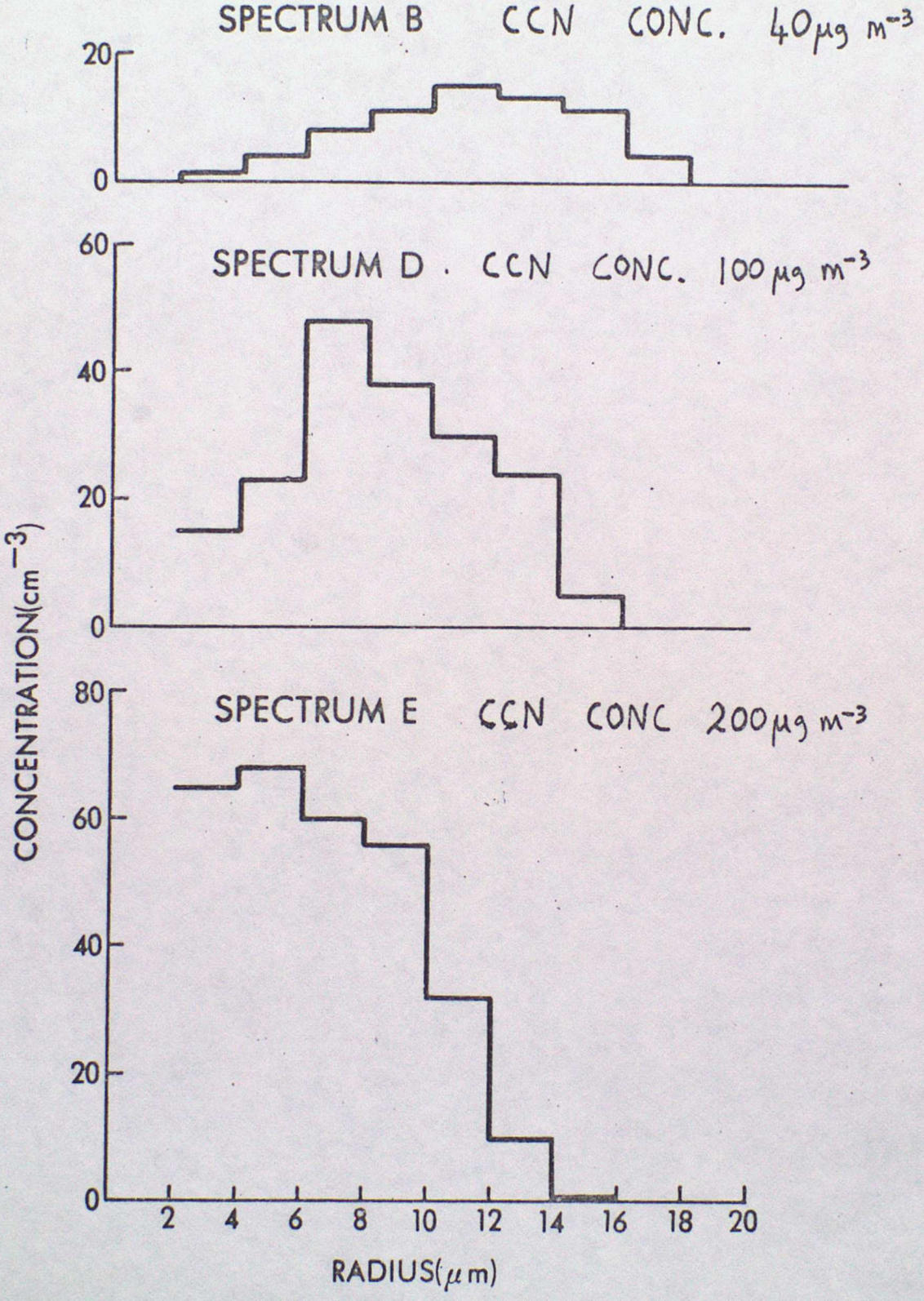

Figure 11 Drop size distributions at a height of 2m after four hours integration. Each distribution is for a different nucleus concentration as annotated.